

Research Article

A Robust EMD-Based RVFL Network Fusion Algorithm for Low-Cost GPS/INS Integrated System

Da Liu , Shufang Zhang , and Jingbo Zhang 

Information Science and Technology College, Dalian Maritime University, Dalian 116026, China

Correspondence should be addressed to Jingbo Zhang; zhang_jingbo@dlnu.edu.cn

Received 28 May 2019; Accepted 1 August 2019; Published 13 October 2019

Academic Editor: Luis Rodolfo Garcia Carrillo

Copyright © 2019 Da Liu et al. This is an open access article distributed under the Creative Commons Attribution License, which permits unrestricted use, distribution, and reproduction in any medium, provided the original work is properly cited.

Global positioning system (GPS) and inertial navigation system (INS) are commonly combined to overcome disadvantages of each and constitute an integrated system that realizes long-term precision. However, the performance of the integrated system deteriorates on which GPS is unavailable. Especially when low-cost inertial sensors based on the microelectromechanical system (MEMS) are used, performance of the integrated system degrades severely over time. In this study, in order to minimize the adverse impact of high-level stochastic noise from low-cost MEMS sensors, denoising technology based on empirical mode decomposition (EMD) is employed to improve signal quality before navigation solution by which significant improvement of removing noise is achieved. Moreover, a random vector functional link (RVFL) network-based fusion algorithm is presented to estimate and compensate position error during GPS outage such that error accumulation is suppressed quickly when INS is working standalone. Performance of the proposed approach is evaluated by experimental results. It is indicated from comparison that the proposed algorithm takes advantages such as better accuracy and lower complexity and is more robust than the commonly reported methods and is more appropriate for real-time and low-cost application.

1. Introduction

Nowadays, navigation technology has attracted more attention than ever before on account of the increasing demand for positioning or location in various fields such as consumer electronics, displacement monitoring, and intelligent transportation. Global navigation satellite system (GNSS) and INS are two main positioning systems with high precision, high performance, and high reliability. GPS as a representative of GNSS has advantages of providing high long-term position accuracy and low cost. However, it suffers from obstruction and interference, leading to giving a continuous navigation solution in an urban canyon. On the contrary, INS could operate continuously with high bandwidth and presents low short-term noise, but its accuracy degrades with time elapse as the inertial instrument errors are accumulated fast. The complementary characteristics of INS and GNSS promote the integration of the two positioning systems, generating a new system possessing a continuous, complete navigation solution with high long- and short-term accuracy.

In the GPS/INS integrated system, Kalman filtering (KF) methods are commonly used for information fusion under assumption that the dynamic statistical model of the system and prior knowledge of the sensors in the system are known which limit the application area and degrade the performance of the system when low-cost sensors are used. Moreover, the accuracy of the integrated system deteriorates significantly on occasion of GPS outage because only the standalone INS system is working which makes the integrated system performance depend on poor long-term accuracy of INS.

To overcome the disadvantages of KF, a kind of effective solution based on an artificial neural network (ANN) is proposed to compensate integrated system deviation caused by GPS blockage, which utilizes the research results of the current popular artificial intelligence (AI). The purpose of applying AI is to bridge the relationship between vehicle motion dynamics and specific information of integrated system by making use of universal approximation capability of the neural networks or other similar models, which is an

intrinsic regression method for fitting a nonlinear function with some signals of the system. Specifically, output data of sensors of the integrated system are employed for training an AI model when GPS is available so that extra information is predicted by a well-trained model to correct the accumulating errors produced by a standalone INS once GPS is blocked. Some scholars have investigated this field and their studies are reported. The radial basis function (RBF) is first introduced to predict position errors between GPS and INS by Sharaf's team [1]. In their work, INS position and time were chosen as network inputs and output was INS error, and wavelet analysis was used to denoise the GPS and INS position signals for network training. In their later work, past samples of INS position and velocity were also utilized as network input to obtain better dynamics performance [2]. On this basis, Chen et al. used dynamical neural network to construct relation between multistep past INS errors and current INS error [3]. Then, Tan et al. developed a new model which combined increments of force and angular velocity rate as model inputs and chose the GPS position increments as model outputs, offering better performance than the traditional INS error output model [4]. Furthermore, Yao et al. selected current speed, specific force, angular velocity, and their past one-step delay as inputs of the multilayer perceptron network to predict GPS incremental output which was the measurement reference for correcting the estimated outputs of KF [5]. All these AI-based methods improved the accuracy of the GPS/INS integrating system in the case of GPS outage.

Various AI algorithms have been applied in compensating the precision loss due to GPS loss for the GPS/INS integrating system, such as the adaptive neuro-fuzzy inference system (ANFIS) [6], support vector machine (SVM) [7–9], feedforward network (FNN) [5], wavelet neural network (WNN) [3], and ensemble learning algorithm [10, 11]. AI-based methods proceeded remarkable prediction improvement in this field. However, they also have disadvantages that cannot be ignored. The parameter optimization process of ANFIS is a time-consuming work so that real-time implementation becomes a difficult task; for SVM, there is no uniform kernel function selection method, training for large samples is slow, and it is sensitive to data loss; the ANN methods including FNN and WNN have drawbacks on the local minimum and overfitting problems, while ensemble learning algorithm like LSBoost or Bagging suffer from disadvantages such as slow convergence and heavy and time-consuming computation. Kinds of new algorithms are proposed to solve these problems, including extreme learning machine (ELM), which is a relatively new method with fast convergence and good generalization ability to train a single-hidden layer feedforward neural network [12]. ELM is a feedforward neural network with single-hidden layer and random weight of hidden nodes, and output weights of ELM are analytically determined instead of being computed by gradient-based learning algorithms. The fast learning speed of ELM makes it suitable for real-time applications. For inertial sensors, especially that are comparatively low cost, preprocessing of the sensor measurements is comparative indispensable. The reason is that reliable data can be extracted from inertial sensor measurements mixed with a high level of stochastic

noise and employed for training of a prediction model so that the model in the prediction mode will offer more actual and accurate output with a lower noise level of the INS data [13]. Wavelet analysis is a commonly efficient tool for signal denoising, which can be facily and effectively implemented in the integrated navigation system to eliminate high-frequency noise via multiresolution features and improve system accuracy [14]. In this background, Abdolkarimi et al. proposed a wavelet-based ELM model to predict INS errors during GPS outage [15]. In their work, the wavelet denoising technique was adopted for improving signal-to-noise power ratio (SNR) of inertial sensor measurements and removing disturbance of high-frequency noise, ELM was used for quick learning and supply faster prediction update, and performance of the proposed model was evaluated in a real-time environment.

In recently reported investigation in the literatures, another feedforward network similar to ELM, termed as RVFL, has been proved possessing better performance in classification and regression issues [16, 17]. RVFL was first proposed to solve systems identification problem [18]. It is a single-hidden layer neural network with random weights and direct input-output connections between input and output neurons. The feature of direct links is the main difference between RVFL and ELM, without which the network may be unstable due to the randomly generated weights between the input and the hidden layer. To acquire superior performance of the GPS/INS integrating system with low-cost inertial sensors in the absence of GPS signal, we focus on the advantages of RVFL and investigate this promising network and evaluate its effectiveness in integrated navigation field. Moreover, a novel denoising method based on EMD was recently proposed to exceed the performance achieved by wavelet analysis [19, 20]. The new method is also complied with thresholding principle, whereas it exhibits better performance in the cases where the signal has a high noise level or high sampling frequency. Motivated by achieving and enhancing continuous high-precision operation performance even during the GPS outages, a novel AI-based methodology for the low-cost INS/GPS navigation system is proposed in this paper to solve the problems existing in the methods mentioned above, in which the high-frequency noise from low-cost sensors are suppressed by EMD denoising technology and high positioning accuracy, and real-time learning capability are obtained by taking advantage of the fast learning of RVFL. In this study, the superior performance of EMD denoising for low-cost inertial sensors is investigated compared to wavelet analysis denoising, and the integrated navigation model and algorithm utilizing RVFL is experimentally evaluated with some existing methods to demonstrate effectiveness and excellent performance of the proposed method.

The rest of this paper is organized as follows: Section 2 concisely describes the INS/GPS integrated navigation system with extended Kalman filter (EKF). Section 3 introduces theoretical details of EMD denoising technology. Section 4 presents an RVFL-based fusion algorithm and overall integration model. Experimental results on field test that verify the proposed methodology are illustrated and discussed in Section 5. Section 6 concludes this work in the end.

2. INS/GPS Integrated Navigation System

In order to take advantage of the complementary characteristics of INS and GNSS, systems combining both technologies are established for a variety of applications. Integrated with GNSS, even low cost INS can be suitable for practical navigation solution. Integration is usually based on a Kalman filter, and INS solution is corrected by GNSS solution to form integration solution.

To describe the vehicle motion dynamics, continuous time state-space equations are constructed as

$$\begin{cases} \dot{\mathbf{x}} = \mathbf{F}(\mathbf{x}) + \mathbf{G}\mathbf{w}, \\ \mathbf{z} = \mathbf{H}\mathbf{x} + \mathbf{r}, \end{cases} \quad (1)$$

where \mathbf{F} denotes the state transition process of the dynamic model which is formulized as nonlinear vehicle motion equations, \mathbf{x} is the state vector whose elements are variable of \mathbf{F} , \mathbf{G} is the system noise matrix, \mathbf{w} and \mathbf{r} are the process and observation noise vector, both of which are supposed to be zero mean white noise. \mathbf{z} represents the observation vector. \mathbf{x} is selected as follows:

$$\mathbf{x} = [\delta\Psi \ \delta v_E \ \delta v_N \ \delta v_U \ \delta L \ \delta\lambda \ \delta h \ \nabla_x \ \nabla_y \ \nabla_z \ \varepsilon_x \ \varepsilon_y \ \varepsilon_z]^T, \quad (2)$$

where $\delta\Psi = [\delta\phi \ \delta\theta \ \delta\psi]$, $\delta\phi$, $\delta\theta$, and $\delta\psi$ are roll, pitch, and yaw errors in the navigation frame (n -frame) in which the x - y - z axes are set as East, North, and Up, respectively. δv_E , δv_N , and δv_U denote vehicle speed errors relative to referential orientation. δL , $\delta\lambda$, and δh are position errors of vehicle resolved as longitude, latitude, and altitude. The subscripts x , y , and z represent the x , y , and z axis of the body frame (b -frame); thus, ∇_x , ∇_y , ∇_z , ε_x , ε_y , and ε_z are expressed as accelerometer and gyros biases along the body-axis.

\mathbf{H} is the measurement model matrix that can be modeled as

$$\mathbf{H} = [0_{3 \times 6} \ \mathbf{I}_{3 \times 3} \ 0_{3 \times 6}], \quad (3)$$

where the subscripts represent the matrix dimension. It is indicated that position variables are chosen as measurements which can be updated by sensors' position information supply.

Matrix \mathbf{F} can be derived from INS navigation error propagation equations, which are formulated as follows [21]:

$$\begin{aligned} \dot{\Psi} &= (\mathbf{I} - \mathbf{C}_{n'}^{n'})\omega_{in}^n + \delta\omega_{in}^n - \mathbf{C}_b^n \delta\omega_{ib}^b, \\ \delta\dot{\mathbf{v}} &= (\mathbf{I} - \mathbf{C}_{n'}^n)\mathbf{C}_b^{n'} \mathbf{f}_{ib}^b + \mathbf{C}_b^n \delta\mathbf{f}_{ib}^b + \delta\mathbf{v} \times (2\omega_{ie}^n + \omega_{en}^n) \\ &\quad + \mathbf{v} \times (2\delta\omega_{ie}^n + \delta\omega_{en}^n), \\ \delta\dot{L} &= \frac{\delta v_N}{R_N + h} - \frac{v_N \delta h}{(R_N + h)^2}, \end{aligned} \quad (4)$$

$$\delta\dot{\lambda} = \frac{\delta v_E \sec L}{R_E + h} + \frac{v_E \tan L \sec L \delta L}{R_E + h} - \frac{\delta h v_E \sec L}{(R_E + h)^2}$$

$$\delta\dot{h} = \delta v_U,$$

where ω_{ba}^c denotes the angular velocity of the a -frame with respect to the b -frame resolved in c -frame. The inertial frame is symbolized with subscript i as i -frame. Likewise, e -frame represents the earth-centered earth-fixed frame. $\mathbf{C}_b^{n'}$ is a transformation matrix from b -frame to actual navigation frame (n' -frame). R_N and R_E are referred as the meridian radius of curvature and the transverse radius of curvature; $\mathbf{C}_{n'}^n$ is a transformation matrix from n -frame to n' -frame which is expressed as

$$\mathbf{C}_{n'}^n = \begin{bmatrix} C\theta C\psi - S\theta S\varphi S\psi & C\theta S\psi + S\theta S\varphi C\psi & -S\theta C\varphi \\ -C\varphi S\psi & C\varphi C\psi & S\varphi \\ S\theta C\psi + C\theta S\varphi S\psi & S\theta S\psi - C\theta S\varphi C\psi & C\theta C\varphi \end{bmatrix}, \quad (5)$$

where C represents the cosine operation and S represents the sine operation. It is obvious that state variables are multiplied so that nonlinear couples exist in the state equations. When attitude angles are small quantities, it is commonly true to consider the system dynamic model is linear. However, if large system uncertainty exists, especially for yaw error, linear assumptions are not valid as a result of the elements coupled in $\mathbf{C}_{n'}^n$ [22]. In this case, KF, which is limited to be only suitable for linear system optimal estimation, is no more an effective fusion algorithm for the integrated navigation system. Therefore, EKF is chosen as the fusion algorithm when GPS is normally working. EKF essentially transforms the nonlinear model to a linear model by Taylor series approximation before applying the KF paradigm. After discretizing the state-space equation (1), first-order EKF is involved in the following two steps.

Prediction:

$$\begin{aligned} \mathbf{x}_{k|k-1} &= f(\mathbf{x}_{k-1}), \\ \mathbf{P}_{k|k-1} &= \mathbf{F}_{k-1}(\mathbf{x}_{k-1})\mathbf{P}_{k-1}\mathbf{F}_{k-1}^T(\mathbf{x}_{k-1}) + \mathbf{Q}_{k-1}. \end{aligned} \quad (6)$$

Update:

$$\begin{aligned} \mathbf{K}_k &= \mathbf{P}_{k|k-1}\mathbf{H}_k^T(\mathbf{H}_k\mathbf{P}_{k|k-1}\mathbf{H}_k^T + \mathbf{R}_k)^{-1}, \\ \mathbf{x}_k &= \mathbf{x}_{k-1} + \mathbf{K}_k\mathbf{H}_k\mathbf{x}_{k|k-1}, \\ \mathbf{P}_k &= [\mathbf{I} - \mathbf{K}_k\mathbf{H}_k]\mathbf{P}_{k|k-1}, \end{aligned} \quad (7)$$

where f is the discretized nonlinear functions from continuous INS navigation error propagation equations. Subscript k denotes the k th epoch in the iteration. \mathbf{P} is the predicted state covariance matrix, \mathbf{Q} and \mathbf{R} are the process and measurement noise covariance matrix, \mathbf{K} is the filter gain matrix, and \mathbf{I} is the identity matrix. The Jacobian matrix \mathbf{F}_k is determined as

$$\mathbf{F}_k = \frac{\delta f(\mathbf{x}_{k-1})}{\delta \mathbf{x}_{k-1}}. \quad (8)$$

3. EMD-Based Denoising

It is necessary to refine raw sensor measurements before applying to the integrated navigation system on account of

the reasons that low-cost inertial sensors have high stochastic noise and highly complex nonlinearity which deteriorate the signal quality and decline the system performance.

As the development of signal-processing technology, a variety of denoising methods are developed such as basing on Fourier transform, short-time Fourier transform, and wavelet transform [15]. A new signal-processing technology termed EMD was developed and researched recently [23]. Signal can be decomposed to a few basic components as intrinsic mode functions (IMFs) via an iterative sifting procedure, the advantages of which are multiresolution analysis ability and free of difficulty in selecting basis. In this background, the signal denoising method based on EMD was proposed to enhance SNR performance, compared to wavelet denoising in a worsened noisy environment [19]. The same principle with thresholding according to wavelet denoising was used in this method, whereas special natures of decomposed signals resulting from EMD were considered to properly choose adaptive thresholding operation to obtain better signal noise reduction. Several denoising procedures were alternative, among which the clear iterative EMD interval-thresholding (EMD-CIIT) was proved to have better performance.

To avoid contaminated signal with the noise integrated navigation system from degrading performance of the integrated navigation system, the EMD-CIIT denoising method is adopted to remove harmful noisy signals for enhancing SNR of the raw measures of inertial sensors which are employed for dead reckoning of INS and training of the neural network, so that the precision of the system is improved. The fundamental procedure of EMD-CIIT is summarized in the following 3 phases.

3.1. Redistributing Noise Signal. This phase is key operation of EMD-CIIT, which has the main difference compared to other EMD-based denoising algorithms such as EMD-IT and EMD-IIT.

- (1) The original noisy signal $x(t)$ is decomposed by EMD to L IMFs: $h_1(t)$, $h_2(t)$, \dots , and $h_L(t)$.
- (2) Extract denoised signal $\tilde{h}_1(t)$ from the first IMF $h_1(t)$ via the thresholding method such as Bayesian wavelet denoising. The purpose of this operation is to avoid contamination results from altering the mixture of the noise signal and useful signal.
- (3) Separating actual noise signal $h_{1(n)}(t)$ from $h_1(t)$,

$$h_{1(n)}(t) = h_1(t) - \tilde{h}_1(t). \quad (9)$$

- (4) Thus, a partial reconstruction signal $x_p(t)$ excluding noise signal in first IMF is obtained:

$$x_p(t) = \sum_{i=2}^L h_i(t) + \tilde{h}_1(t). \quad (10)$$

- (5) Generate new noisy versions of the origin noisy signal by adding modified versions of $h_{1(n)}(t)$ whose sample positions are randomly altered.

$$x_a(t) = x_p(t) + h_{1(a)}(t), \quad (11)$$

where $h_{1(a)}(t)$ is the altered version of $h_{1(n)}(t)$ and the relationship is expressed as

$$h_{1(a)}(t) = \text{alter}(h_{1(n)}(t)), \quad (12)$$

in which the alter function often deals with the samples of $h_{1(n)}(t)$ in two forms: random circulation or random permutation.

3.2. Thresholding Denoising

- (6) Apply EMD expansion on $x_a(t)$ to generate IMFs.
- (7) Employ EMD soft thresholding to process each IMF of $x_a(t)$ and get a denoised version $\tilde{x}_1(t)$ of $x(t)$, which is formulized as

$$\tilde{h}^{(i)}(z_j^{(i)}) = \begin{cases} h^{(i)}(z_j^{(i)}) \frac{|h^{(i)}(r_j^{(i)})| - T_i}{|h^{(i)}(r_j^{(i)})|}, & |h^{(i)}(r_j^{(i)})| > T_i, \\ 0, & |h^{(i)}(r_j^{(i)})| \leq T_i, \end{cases} \quad (13)$$

where $h^{(i)}(z_j^{(i)})$ is referred as the z th interval of the i th IMF component which is divided by zero crossings, and $h^{(i)}(r_j^{(i)})$ denotes the single extrema correspond to this interval. T_i is an adaptive threshold depended on the noise level and is commonly determined as $\sigma\sqrt{2\ln N}$, where N is the sample length and σ is the standard deviation of the noise and can be empirically estimated.

In actual application, some low-order IMFs are excluded of reconstruction for flexibility and rationality which are handled empirically, and for more details, refer to [19].

- (8) Iterate $k-1$ times from Steps (5) to (7) and obtain different k denoised versions of $x(t)$, i.e., $\tilde{x}_1(t)$, $\tilde{x}_2(t)$, \dots , $\tilde{x}_k(t)$.

3.3. Obtaining Denoised Signal

- (9) Calculate the average of each denoised version of $x(t)$ to get final denoised results of the origin signal.

$$\tilde{x}(t) = \frac{1}{k} \sum_{i=1}^k \tilde{x}_i(t). \quad (14)$$

After completing the denoising process between Phase 1 and Phase 3, refined signals of inertial sensors with higher SNR are obtained that are more suitable for the next prediction.

4. Integrated System Based on RVFL

As mentioned above, RVFL is a single layer feedforward neural network (SLFN) with fast training algorithm, having

favorable features on overfitting, local minima, and generalization, which is attributed to the characteristic network structure illustrated in Figure 1.

In the input layer, M selected features are fed into the input layer neurons where x_1, \dots, x_M represent the elements of the input vector and i_1, \dots, i_M represent M input neurons. The input layer neurons do not change information from the input of the network and only serve as transfer nodes, that is

$$i_m = x_m, \quad (15)$$

where $m \in \{1, \dots, M\}$ represents the m th of all M elements.

In the hidden layer, each of the hidden layer neurons h_n , $n \in \{1, \dots, N\}$, also known as enhancement nodes, takes the weighted sum of all the output of the input layer neurons and generates its output via an activation function:

$$h_n = f\left(\sum_{m=1}^M w_{mn}i_m + b_n\right), \quad (16)$$

where w_{mn} is the connected weight between i_m and h_n , b_n is the bias of the n th hidden layer neuron, and $f(\cdot)$ is a nonlinear function in which radial basis transfer function is employed as

$$f(x) = e^{-x^2}. \quad (17)$$

In the output layer, neurons combine all the output of hidden layer neurons according to interconnected weight between every hidden layer neuron and output layer neuron; besides, output from the input layer are also weighted summed to the output layer neurons, and the output is

$$y_l = o_l = \sum_{n=1}^N w_{nl}h_n + \sum_{m=1}^M w_{ml}i_m, \quad (18)$$

where $l \in \{1, \dots, L\}$, L is the number of output, y_l is l th output which is equal to the output of the l th output layer neuron, i.e., o_l , w_{nl} is the connected weight between h_n and o_l , and w_{ml} is the connected weight between i_m and o_l .

The structure of RVFL is similar as normal SLFN except the direct link from the input layer to the output layer. This special character makes RVFL perform better and stable compared to no direct link [16, 17]. Moreover, for RVFL, the weights from input neurons to hidden neurons such as w_{mn} , and hidden layer biases such as b_n , are assigned fixed random values, which is usually in accordance with uniform distribution in a determined range. As a result, the network does not have to turn and update parameters during training by back propagation (BP) algorithm which is time-consuming, heavy computing burden, and prone to local minimization; on the contrary, it is able to proceed the training process on ‘‘one step’’, by solving the linear optimal problem. The relationship of input and output can be formalized as

$$\mathbf{T} = \mathbf{O} = \mathbf{A}\boldsymbol{\beta}, \quad (19)$$

where $\mathbf{A} = [\mathbf{H}, \mathbf{I}]$ represents the augmented matrix comprising of output of hidden layer and input layer, \mathbf{T} is the

actual output vector, \mathbf{O} is the expected optimized output vectors of RVFL aiming to minimize squared error between prediction and actual output in the learning stage, and $\boldsymbol{\beta}$ represents the output weights which can be mathematically solved. To obtain the optimal solution, Moore–Penrose pseudoinverse matrix is commonly used such that the output weights can be derived as

$$\boldsymbol{\beta} = \mathbf{A}^+\mathbf{T}, \quad (20)$$

where \mathbf{A}^+ is the Moore–Penrose pseudoinverse matrix of matrix \mathbf{A} . There is another alternative method called ridge regression that may provide better performance for RVFL than the Moore–Penrose pseudoinverse matrix method. The solution of ridge regression is

$$\boldsymbol{\beta} = \mathbf{A}(\mathbf{A}^T\mathbf{A} + \lambda\mathbf{I})^{-1}\mathbf{T}, \quad (21)$$

where λ is a turned regularization parameter. In this way, parameters of RVFL are determined much faster than those of BP on account of processing combination of original features and random features and target output in batch mode.

In this work, RVFL is utilized to bridge the discontinuous navigation course during the GPS outage by means of predicting the accuracy position information. There are a few basic input-output models reported in literature which can be divided into several classes. One of these models is called $\mathbf{O}_{\text{INS}} - \delta\mathbf{P}_{\text{INS}}$, the which utilizes output of INS to predict the INS error compared to GPS and other kinds of models called $\mathbf{O}_{\text{INS}} - \mathbf{X}_k$ directly to predict the state vector involved in KF. Both of the models take the output of KF as the network target; as a result, the prediction is intended to be affected by the uncertain estimated error of KF which may be accumulated to larger error, especially when low-cost inertial sensors are used in the system. Therefore, a model is developed recently termed as $\mathbf{O}_{\text{INS}} - \Delta\mathbf{P}_{\text{GPS}}$ that selects GPS incremental output as a target by which the network prediction is no longer influenced by the past filtered results of KF. Hence, an RVFL-based GPS incremental prediction model is proposed to realize the AI-aided integrated navigation system. This model works in two modes which are training and predicting, respectively, illustrated in Figures 2 and 3.

Figure 2 shows the integrated system is operating in the training mode when GPS signal is available. An inertial measurement unit (IMU) with 6 degrees of freedom (DOF) supplies three axes accelerator and three axes gyro origin measurement output, which are denoised by the EMD-CIIT method in the next step to generate cleaner signal with higher SNR. \mathbf{f} and $\boldsymbol{\omega}$ denote the original specific force vector and original angular rate vector, respectively, comprising three components resolved in the body frame. $\hat{\mathbf{f}}$ and $\hat{\boldsymbol{\omega}}$ are the denoised version of \mathbf{f} and $\boldsymbol{\omega}$. With the inertial measurement input, the attitude, velocity, and position information, i.e., $\boldsymbol{\Psi}_{\text{INS}}$, \mathbf{v}_{INS} , and \mathbf{P}_{INS} , are obtained in the way of applying inertial mechanization equations in INS. Then, the output information of INS and position information of GPS are fused in a loosely couple architecture via EKF, in which the deviation of INS increasing over time are

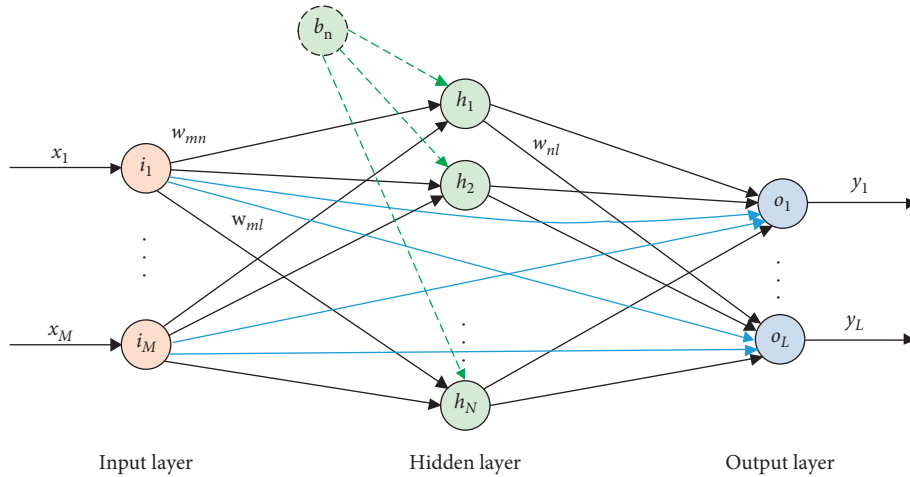


FIGURE 1: RVFL network structure.

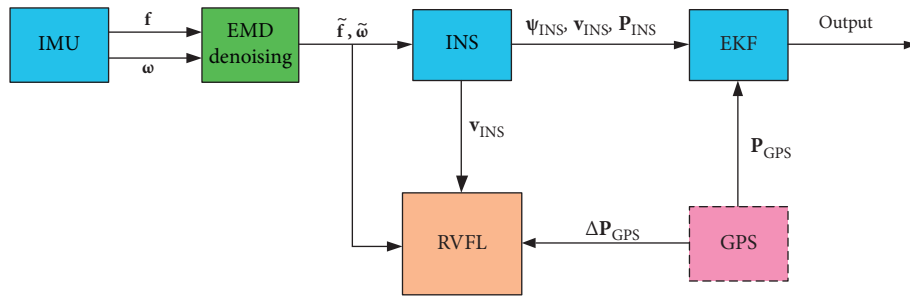


FIGURE 2: EMD-based RVFL integration scheme in training mode.

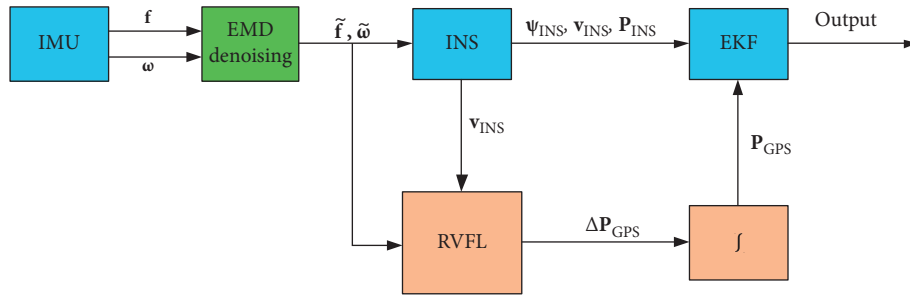


FIGURE 3: EMD-based RVFL integration scheme in predicting mode.

corrected by GPS information in fixed time steps such that the integrated navigation system becomes relatively stable and accurate. Meanwhile, the velocity of INS and denoised inertial measurement are fed into RVFL as input features, and the GPS increment ΔP_{GPS} is chosen as the target of RVFL. The training process establishes a non-linear relationship between the inertial inputs and GPS increment position by taking advantage of input and output data to determine network parameters. Hence, the trained RVFL holds the predicting character, and it is a backup for harsh environment or situation on which GPS is unavailable.

When the GPS signal has been blocked in a worse urban environment, the integrated system is switched into the

predicting mode, which is illustrated in Figure 3. In this working mode, unreliable GPS information is abandoned and no more employed to the integration of EKF, instead, RVFL is utilized to correct INS errors. RVFL takes inertial signals as input which is the same as that in the training mode. Input signals are processing in real time in RVFL, and the network output is “quasi-GPS incremental position” that is used as a substitution output of GPS. Therefore, EKF combines the outputs of INS and prediction of RVFL to generate new integrated navigation output. In other words, the INS errors that have been corrected by GPS are compensated via RVFL so that the navigation outputs will diverge from the actual position much slower compared to standalone INS.

5. Experimental Results and Discussion

5.1. Experimental Technical Description. To evaluate and verify performance of the proposed integrated navigation system, field experiment is conducted in Dalian, Liaoning Province, China. The duration of the experiment is 2400 s, and the driving trajectory of the vehicle with navigation equipment is shown with colored line in Figure 4. The marked red line denotes simulated GPS outage in which different driving dynamics are considered. In actual application, whether GPS is available needs to be determined. An effective method is to estimate whether GPS signals are direct LOS according to carrier-power-to-noise-density ratio [24].

Navigation equipment including low-cost MEMS-based IMU, GPS receiver, and attitude and heading reference system (AHRS) were mounted inside an electric automobile. The IMU consists of three accelerators and three gyros which are produced via MEMS technology characterized on low cost as well as lower precision and works at 100 Hz sampling rate to generate raw specific force and angular rate measurements. The information of specified technical parameters is listed in Table 1. A GPS receiver which has 0.1 m/s speed accuracy, 2.5 m position accuracy, and 5 Hz update rate was employed to constitute the loosely couple integrated navigation system with IMU. In order to provide a reference for the proposed system, an AHRS with static accuracy of 0.1° , dynamic accuracy of 0.5° , and resolution of 0.1° was used in the experiment.

As shown in Figure 5, the sensors contained in IMU, i.e., accelerators and gyros, output raw measures of specific force, and angular rate, respectively, which are combined in binary data steam in the SPI interface to be sent to an embedded system based on the STM32F405 processor. The GPS receiver also sends measurements and monitor status information formatted as NEMA messages in the UART interface with a baud rate of 115200. The embedded system is composed of an ARM processor and peripheral circuits, and it is used to process signal from inertial sensors and extract position information from data of the GPS receiver. All the processed data to be used for the proposed algorithm are transmitted by an RS232 serial port from the embedded system to host computer in which robust integrated navigation algorithm is implemented. Meanwhile, AHRS is connected to the host to supply referential position and attitude information.

5.2. Performance Improvement of Applying EMD Denoise. To suppress the effect of noise on the system, a denoise method based on EMD mentioned above is utilized to refine the output signals of INS such as specific force and angular rate. The filtered parameters are determined as iterations number is 5, sifting number is 10, and soft thresholding is applied.

Figure 6 shows the result of denoised signals compared to raw signals during experiment time from 400 s to 900 s, where f and ω with subscript denote specific force and angular rate resolve in the body frame, respectively. The

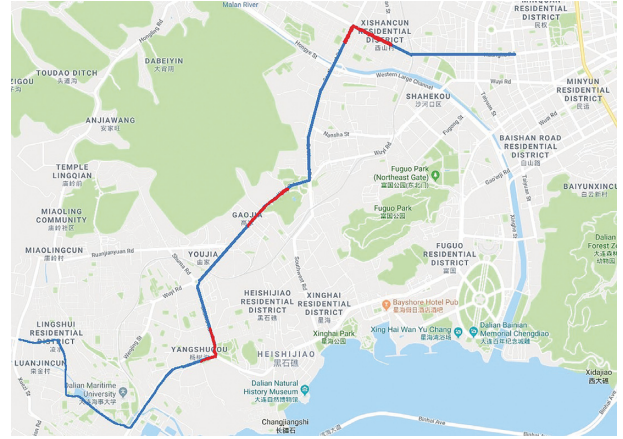


FIGURE 4: Navigation trajectory.

TABLE 1: IMU parameter characteristics.

| Parameter | Accelerometer | Gyroscope |
|-----------------------|-------------------------------------|--|
| Range | ± 2 g | $\pm 1000^\circ$ (s) |
| In-run bias stability | 5 mg | 50° (h) |
| Noise density | $110 \mu\text{g}(\sqrt{\text{Hz}})$ | $0.005^\circ(\text{s}/\sqrt{\text{Hz}})$ |
| Misalignment error | 0.05° | 0.05° |
| Nonlinearity | 0.5% | 0.2% |
| Axis alignment | 0.05° | 0.05° |

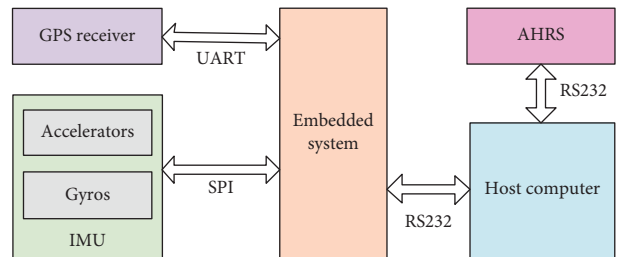


FIGURE 5: System deployment.

specific force and angular rate comparisons are listed in the left and right columns on top, middle, and bottom, respectively. The raw and denoised signals in each subfigure are indicated in blue and red lines.

From the results illustrated in the figure, it is concluded that most of the high-frequency noise in the processed signals is removed, which comes from intrinsic electrical characteristics of inertial sensors and external vibration. In application, some of the high-frequency noise could be smoothed in the integrating process of dead reckon; however, in a dynamical motion, the noise will not be averaged out to the same extent which leads to the errors in solution. Therefore, it is necessary to denoise signals of sensors before inertial navigation computation. In addition, fast responses of denoised signals are also shown, indicating that useful dynamics containing important motion information is retained that is significant for navigation as well.

Table 2 lists the SNR of various signals on condition of being original and denoised versions which adopt different

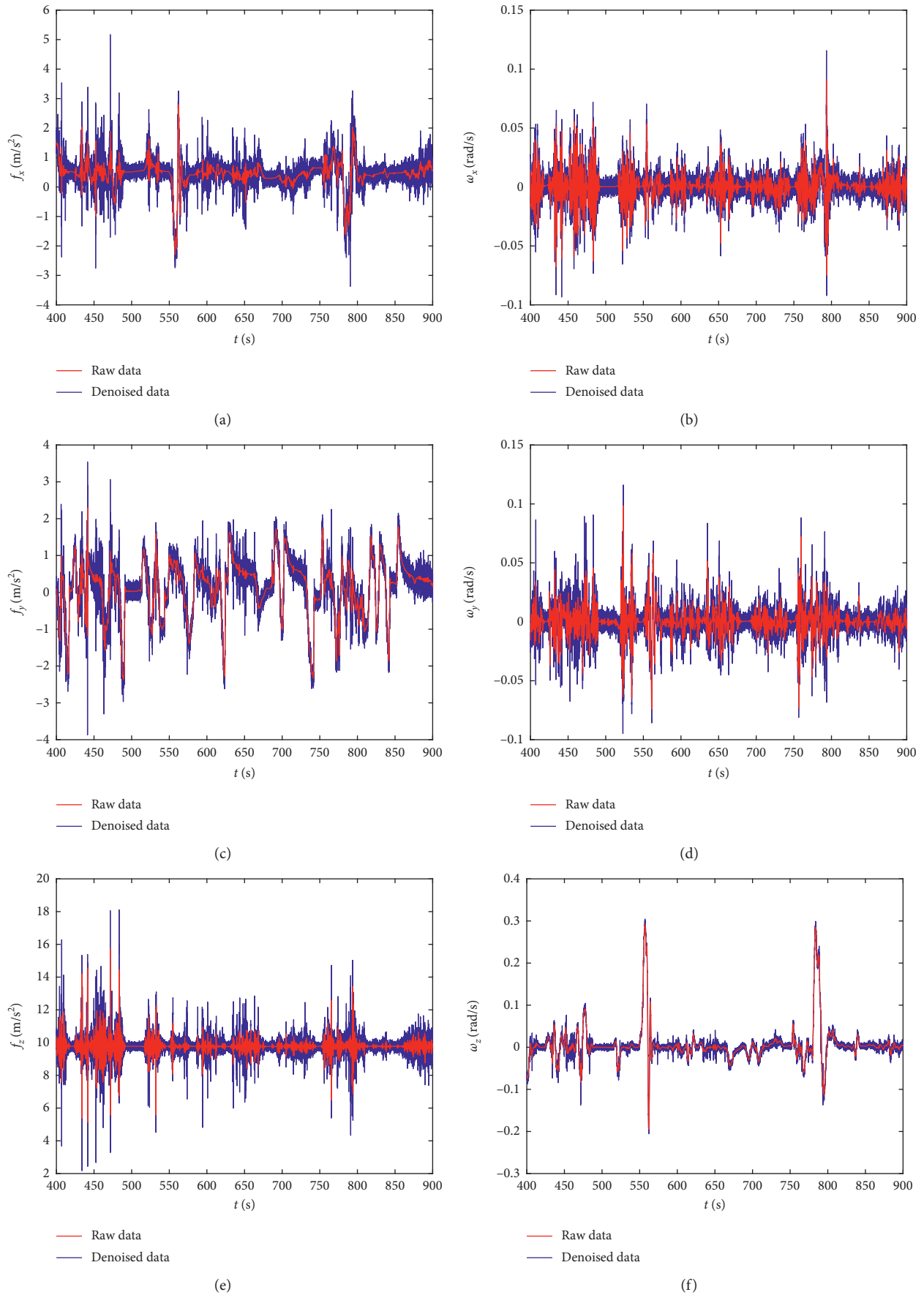


FIGURE 6: Comparison of raw and denoised specific force and angular rate resolved in body frame along x -, y -, z -axes. (a) Specific force resolved along x -axis. (b) Angular rate resolved along x -axis. (c) Specific force resolved along y -axis. (d) Angular rate resolved along y -axis. (e) Specific force resolved along z -axis. (f) Angular rate resolved along z -axis.

TABLE 2: SNR comparison on raw signal and denoised signal based on different methods.

| Parameter | f_x | f_x | f_x | ω_x | ω_y | ω_z |
|------------------|--------|-------|--------|------------|------------|------------|
| Raw signal | -11.38 | -2.29 | -17.31 | -10.36 | -12.78 | -5.74 |
| Wavelet denoised | -10.25 | -1.99 | -14.25 | -9.83 | -12.42 | -5.37 |
| EMD denoised | -5.18 | -1.47 | -10.78 | -9.37 | -11.6 | -4.85 |

denoising methods such as wavelet transform and EMD; in this way, it is evident to further evaluate the effectiveness of EMD-based denoising.

It can be seen from the results that the EMD-based method performs better than the wavelet-based method which also improves the SNR of raw signals. Moreover, the EMD-based method gives better performance especially when the raw signals are with lower SNR. As a result, EMD is a fairly promising denoising method for MEMS-based sensors in some harsh conditions with disturbance and interference.

After denoising, the refined measurements of sensors are used as input signals of inertial navigation so that more accurate and reliable solution could be obtained. Besides the advantage of denoising for INS, it is also conducive for the prediction of neural network because cleaner data are provided for the network to adapt to the real dynamics; as a result, the well-trained network tends to offer more precise estimation results and enhance the robust performance of the system.

5.3. Performance Evaluation of the Proposed Algorithm.

In this study, the proposed model and algorithm are evaluated in different dynamics under urban traffic condition, as depicted in Figure 4, where the red line denotes three simulated GPS outage sections. These sections are distributed in whole trajectory on time interval from 750 s to 870 s, 1450 s to 1570 s, and 1950 s to 2070 s, respectively, which are expressed as outage 1, outage 2, and outage 3. Outage 1 and outage 3 obviously contains change of vehicle motion in north and east directions, respectively, whereas outage 2 illustrates slow position changing of the experimental vehicle, so that fully dynamic conditions are considered.

Figure 7 shows the experiment results tested in outage 1 using different methods. The position errors produced by the navigation system without prediction and compensation, i.e., a standalone INS, are plotted with black line as basic reference. Blue dashed line and red dashed-dotted line, respectively, represent the position error of the system applying ELM and RVFL. For both the predicting algorithms, the train and test data sets of both networks are kept for the same; besides that the network parameters are also identically turned.

It can be seen from the results that, both in north and east directions, the proposed RVFL-based method has best performance among all the candidates, the pure INS has worst performance which exhibits largest position deviation, and the ELM method has worst performance than RVFL but better than the pure INS. Especially for east direction, rapid change takes place at 780 s and INS error increased quickly leading to large deviation from true position, while errors of

ELM and RVFL presented lower increase. The reason pure INS performs much worse than the other two methods is that when INS is working alone without correction of GPS information, the accuracy of the navigation system is only depended on the performance of low-cost MEMS inertial sensors which is fairly sensitive to inherent in-run bias stability and drift; therefore, errors are quickly accumulated over time such that significant deviation of estimated position arises from GPS outage. It is obvious that RVFL outperforms ELM in the outage section. Compared to ELM, besides the same basic feedforward network structure, RVFL adds directly connections from the input layer to the output layer by which the network becomes more stable that of no links due to discrimination power of input features are increased. As a result, both north and east position errors of RVFL are smaller than those of ELM. It can be noted that the errors of the three methods have bias from zero at first when outage occurs, and this is caused by limited precision of INS/GPS integrated system which has errors as well.

North and east position errors for outages 2 and 3 are illustrated in Figures 8 and 9. Outage 2 and outage 3, respectively, represent the vehicle dynamic condition on gradual change of position and rapid change in north. It can be seen from the result that similar performance for the three methods as that in outage 1 is obtained; moreover, the analysis is the same as well.

To further evaluate performance of the proposed RVFL algorithm, Table 3 gives the root mean square error (RMSE) results of outages 1–3 in north and east, respectively. RMSE increasing from top to bottom for each column indicates identical consequence as that of Figures 7–9. The effectiveness of the proposed RVFL method is demonstrated by the result that performance improvement on error reduction in comparison with the pure INS and ELM approach is obtained. It proves that RVFL has superior capability than the other methods to realize accurate and robust navigation in various road dynamic test conditions.

Performance evaluation on RVFL and common neural network such as radial basis function network is also conducted. The radial basis function network (RBN) is a popular feedforward artificial neural network that uses radial basis functions as activation functions and is widely used in the field of function approximation, time series prediction, classification, system control, and so on. The RBN has good capability of generalization, approximation accuracy, and fast convergence speed; moreover, it can adaptively adjust number neurons to satisfy required accuracy of the model. RVFL and RBN are compared in east position error for outage 1, the result of which is shown in Figure 10, and the errors of the RVFL and RBN are depicted with a red line and a green line. In comparison, it is obvious that the RVFL has smaller position error than the RBN, which is clearer when

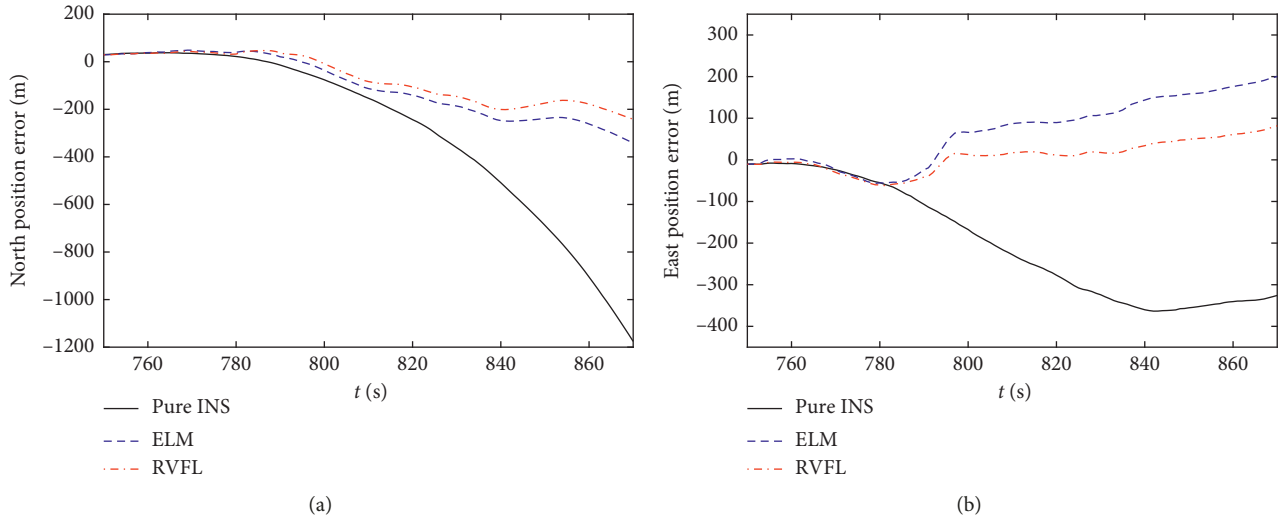


FIGURE 7: Position errors comparison for outage 1. (a) North position errors of INS, ELM, and RVFL. (b) East position errors of INS, ELM and RVFL.

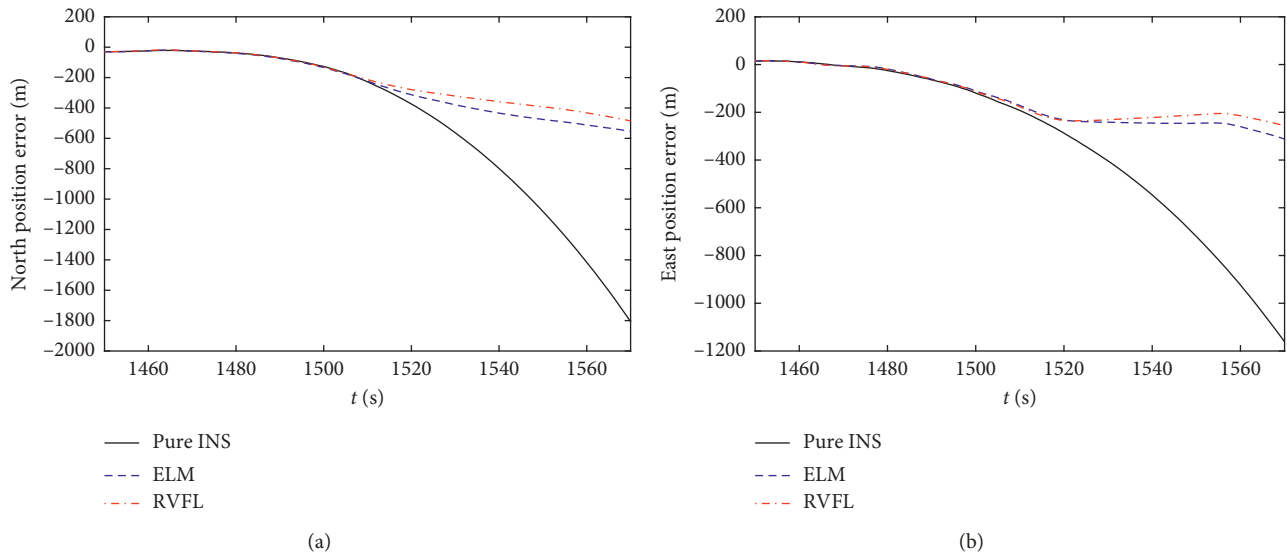


FIGURE 8: Position errors comparison for outage 2. (a) North position errors of INS, ELM, and RVFL. (b) East position errors of INS, ELM, and RVFL.

the vehicle is on dynamic change after 780 s. So it can be concluded that the RVFL outperforms the RBN in high dynamics for the integrated navigation system.

Conclusions obtained above are also confirmed by RMSE results in Table 4. This table lists RMSE for different methods in north and east directions, respectively. Moreover, time consumption of each algorithm is also compared, on host computer configuration of Intel i7-6700CPU@ 3.40 GHz, 4G RAM. As shown in the table, the RVFL has best accuracy compared to the RBN and ELM and achieves faster learning than RBN, which is due to the special parameter determination method by solving linear matrix equation instead of BP. Hence, it is promising to employ RVFL in the integrated navigation system because of not only outstanding capability of nonlinear approximation in

complex dynamic environments suffering from the GPS blockage but also fast response that is important for real-time implementation.

The RMSE of north position error for RVFL and ELM in outage 1 is computed on different noise levels to further prove the effectiveness of EMD denoising. Before denoising, measurements of MEMS-based inertial sensors are fully mixed with stochastic noise, which are used for navigation solution, and RMSE of east position error for ELM and RVFL are 219.7 and 90.3. When EMD denoising is used for raw measurements of sensors, refined input signals are utilized for the prediction model such that more reliable data are used in training and prediction process to produce more actual position estimation results. Denoised results are listed in Table 3, in which RMSE of east position error for ELM and

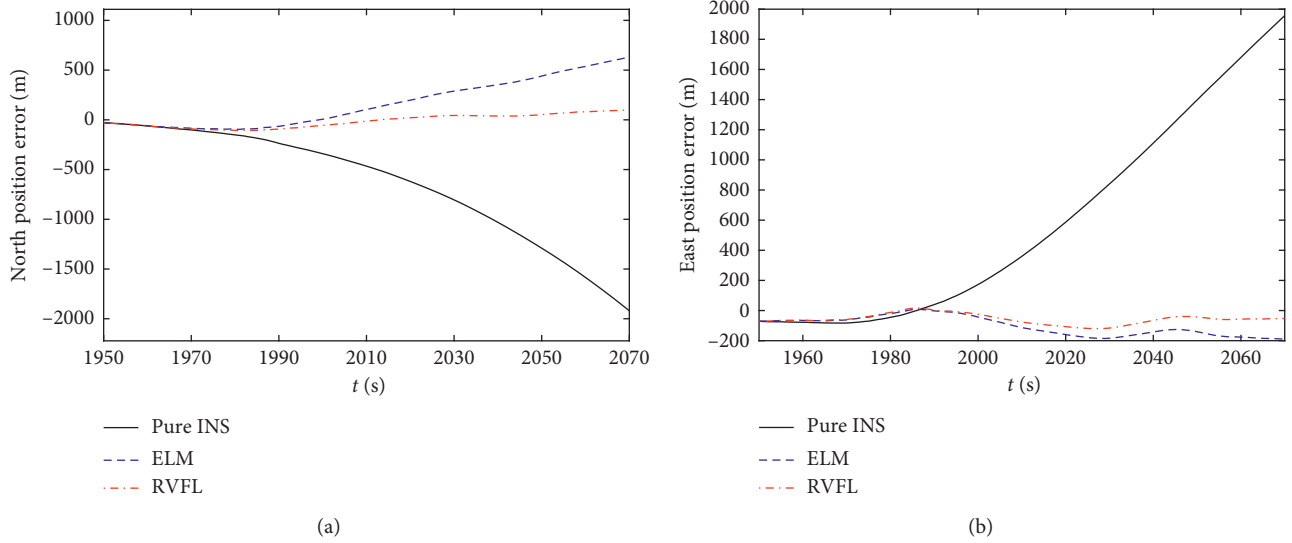


FIGURE 9: Position errors comparison for outage 3. (a) North position errors of INS, ELM, and RVFL. (b) East position errors of INS, ELM, and RVFL.

TABLE 3: RMSE comparison for different outages.

| | Outage 1 | | Outage 2 | | Outage 3 | |
|----------|----------|-------|----------|-------|----------|-------|
| | North | East | North | East | North | East |
| Pure INS | 455.1 | 258.6 | 710.4 | 466.2 | 843.6 | 876.9 |
| ELM | 166.5 | 71.3 | 310.8 | 177.6 | 288.6 | 123.1 |
| RVFL | 122.1 | 45.1 | 266.4 | 166.5 | 66.7 | 66.0 |

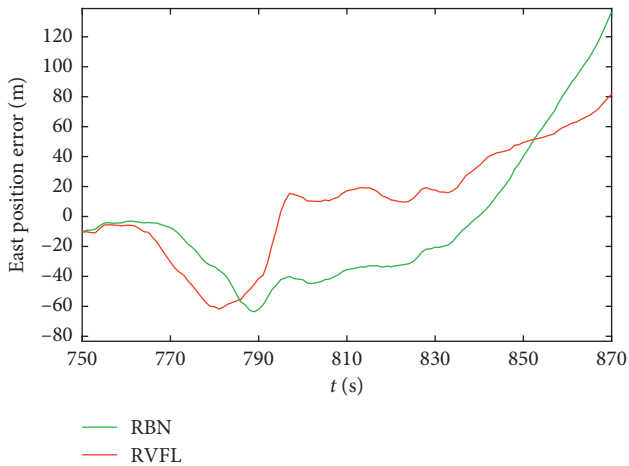


FIGURE 10: Position errors comparison of RVFL and RBN for outage 1.

TABLE 4: RMSE comparison for different methods in outage 1.

| | North | | East | |
|------|-------|----------|------|----------|
| | RMSE | Time | RMSE | Time |
| RBN | 255.3 | 0.099314 | 60.4 | 0.076550 |
| ELM | 166.5 | 0.015102 | 71.3 | 0.010056 |
| RVFL | 122.1 | 0.016556 | 45.1 | 0.01223 |

RVFL are 71.3 and 45.1, respectively. Hence, 67.5% and 50.1% error reduction are achieved for ELM and RVFL after applying EMD denoising, which shows significant performance improvement. According to the comparison, it is evident to prove advantage of denoising technology in improving accuracy of the system.

6. Conclusions

In order to improve accuracy of the GPS/INS integrated navigation system based on low-cost MEMS sensors characterizing high level of noise and complex error, an RVFL-based fusion algorithm is proposed to provide continuous, stable, and robust navigation service even in GPS outage circumstances. In the proposed integrated navigation system, EMD denoising technology is used to smooth high stochastic noise such that the negative effect of disturbance is minimized. In addition, a position incremental model is utilized together with RVFL to adaptively establish relationship between some output of inertial sensors and position increment such that the error of INS can be predicted and compensated during GPS blockage. Solutions of GPS, which are superseded by those of the RVFL model when GPS is unavailable, and outputs of INS are integrated by EKF to generate actual navigation outputs against nonlinear characteristics of the system. A field test is carried

out to demonstrate the effectiveness of the proposed model, and the superior improvement is verified by experiment that the RVFL-based method obtains best accuracy among the algorithms being compared and needs less time to train and predict the process which is proved to be more suitable for implementation in the system requiring real-time operation and low-cost design.

Data Availability

The data used to support the findings of this study are available from the corresponding author upon request.

Conflicts of Interest

The authors declare that there are no conflicts of interest regarding the publication of this paper.

Acknowledgments

This research was funded by the Chinese National Science Foundation (grant nos. 61601078, 61501078, and 61231006), Doctoral Start-Up Foundation of Liaoning Province (grant no. 20170520091), Natural Science Foundation of Liaoning Province (grant no. 20180550964), and Fundamental Research Funds for the Central Universities (grant nos. 3132017073 and 017190327).

References

- [1] R. Sharaf, A. Noureldin, A. Osman, and N. El-Sheimy, "Online INS/GPS integration with a radial basis function neural network," *IEEE Aerospace and Electronic Systems Magazine*, vol. 20, no. 3, pp. 8–14, 2005.
- [2] A. Noureldin, A. El-Shafie, and M. Bayoumi, "GPS/INS integration utilizing dynamic neural networks for vehicular navigation," *Information Fusion*, vol. 12, no. 1, pp. 48–57, 2011.
- [3] X. Chen, C. Shen, W.-B. Zhang, M. Tomizuka, Y. Xu, and K. Chiu, "Novel hybrid of strong tracking Kalman filter and wavelet neural network for GPS/INS during GPS outages," *Measurement*, vol. 46, no. 10, pp. 3847–3854, 2013.
- [4] X. Tan, J. Wang, S. Jin, and X. Meng, "GA-SVR and pseudo-position-aided GPS/INS integration during GPS outage," *Journal of Navigation*, vol. 68, no. 4, pp. 678–696, 2015.
- [5] Y. Yao, X. Xu, C. Zhu, and C.-Y. Chan, "A hybrid fusion algorithm for GPS/INS integration during GPS outages," *Measurement*, vol. 103, pp. 42–51, 2017.
- [6] W. Abdel-Hamid, A. Noureldin, and N. El-Sheimy, "Adaptive fuzzy prediction of low-cost inertial-based positioning errors," *IEEE Transactions on Fuzzy Systems*, vol. 15, no. 3, pp. 519–529, 2007.
- [7] X. Chen, Y. Xu, Q. Li, J. Tang, and C. Shen, "Improving ultrasonic-based seamless navigation for indoor mobile robots utilizing EKF and LS-SVM," *Measurement*, vol. 92, pp. 243–251, 2016.
- [8] X. Li, Q. M. Xu, C. Y. Chan, B. Li, W. Chen, and X. Song, "A hybrid intelligent multisensor positioning methodology for reliable vehicle navigation," *Mathematical Problems in Engineering*, vol. 2015, Article ID 176947, 13 pages, 2015.
- [9] Z. Xu, Y. Li, C. Rizos, and X. Xu, "Novel hybrid of LS-SVM and Kalman filter for GPS/INS integration," *Journal of Navigation*, vol. 63, no. 2, pp. 289–299, 2010.
- [10] J. Li, N. Song, G. Yang, M. Li, and Q. Cai, "Improving positioning accuracy of vehicular navigation system during GPS outages utilizing ensemble learning algorithm," *Information Fusion*, vol. 35, pp. 1–10, 2017.
- [11] H. M. Georges, D. Wang, and Z. Xiao, "GNSS/low-cost MEMS-INS integration using variational Bayesian adaptive cubature Kalman smoother and ensemble regularized ELM," *Mathematical Problems in Engineering*, vol. 2015, Article ID 682907, 13 pages, 2015.
- [12] G. B. Huang, Q. Y. Zhu, and C. K. Siew, "Extreme learning machine: theory and applications," *Neurocomputing*, vol. 70, no. 1–3, pp. 489–501, 2006.
- [13] A. El-Shafie, A. Najah, and O. A. Karim, "Amplified wavelet-ANFIS-based model for GPS/INS integration to enhance vehicular navigation system," *Neural Computing & Applications*, vol. 24, no. 7–8, pp. 1905–1916, 2014.
- [14] T. Zhang and X. Xu, "A new method of seamless land navigation for GPS/INS integrated system," *Measurement*, vol. 45, no. 4, pp. 691–701, 2012.
- [15] E. S. Abdolkarimi, G. Abaei, and M. R. Mosavi, "A wavelet-extreme learning machine for low-cost INS/GPS navigation system in high-speed applications," *GPS Solutions*, vol. 22, no. 1, 2018.
- [16] L. Zhang and P. N. Suganthan, "A comprehensive evaluation of random vector functional link networks," *Information Sciences*, vol. 367–368, pp. 1094–1105, 2016.
- [17] Y. Ren, P. N. Suganthan, N. Srikanth, and G. Amaratunga, "Random vector functional link network for short-term electricity load demand forecasting," *Information Sciences*, vol. 367–368, pp. 1078–1093, 2016.
- [18] Y.-H. Pao, S. M. Phillips, and D. J. Sobajic, "Neural-net computing and the intelligent control of systems," *International Journal of Control*, vol. 56, no. 2, pp. 263–289, 1992.
- [19] Y. Kopsinis and S. McLaughlin, "Development of EMD-based denoising methods inspired by wavelet thresholding," *IEEE Transactions on Signal Processing*, vol. 57, no. 4, pp. 1351–1362, 2009.
- [20] L. Ke, "Denoising GPS-based structure monitoring data using hybrid EMD and wavelet packet," *Mathematical Problems in Engineering*, vol. 2017, Article ID 4920809, 7 pages, 2017.
- [21] P. D. Groves, *Principles of GNSS, Inertial, and Multisensor Integrated Navigation Systems*, Artech House, Norwood, MA, USA, 2013.
- [22] B. Cui, X. Chen, Y. Xu, H. Huang, and X. Liu, "Performance analysis of improved iterated cubature Kalman filter and its application to GNSS/INS," *ISA Transactions*, vol. 66, pp. 460–468, 2017.
- [23] N. E. Huang, Z. Shen, S. R. Long et al., "The empirical mode decomposition and the Hilbert spectrum for nonlinear and non-stationary time series analysis," *Proceedings of the Royal Society A-Mathematical Physical and Engineering Sciences*, vol. 454, no. 1971, pp. 903–995, 1998.
- [24] M. Adjrad and P. D. Groves, "Intelligent urban positioning: integration of shadow matching with 3d-mapping-aided GNSS ranging," *Journal of Navigation*, vol. 71, no. 1, pp. 1–20, 2018.



Hindawi

Submit your manuscripts at
www.hindawi.com

